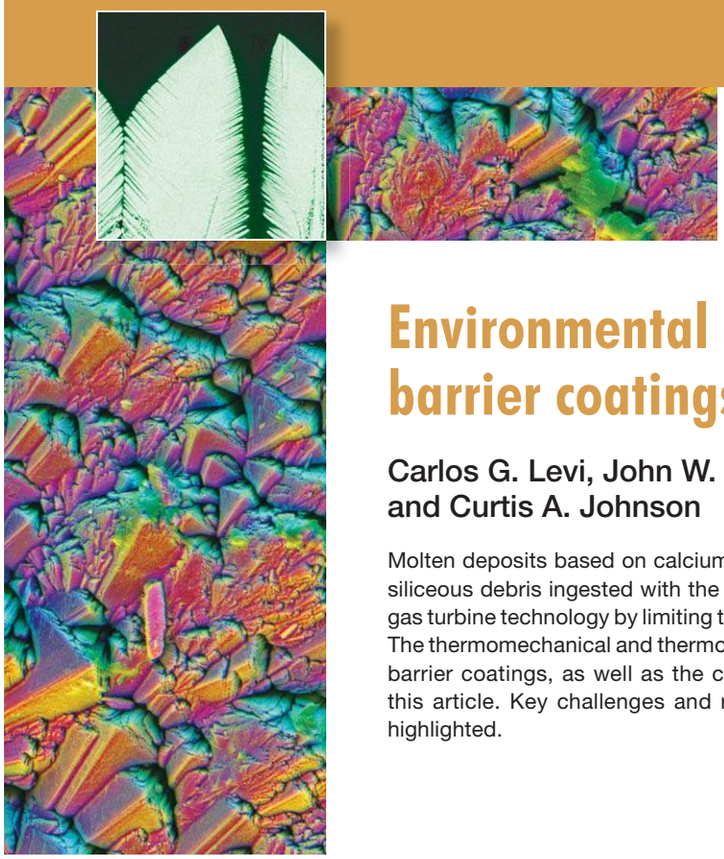

Environmental degradation of thermal-barrier coatings by molten deposits

Carlos G. Levi, John W. Hutchinson, Marie-Hélène Vidal-Sétif, and Curtis A. Johnson

Molten deposits based on calcium-magnesium alumino-silicates (CMAS), originating from siliceous debris ingested with the intake air, represent a fundamental threat to progress in gas turbine technology by limiting the operating surface temperature of coated components. The thermomechanical and thermochemical aspects of the CMAS interactions with thermal-barrier coatings, as well as the current status of mitigating strategies, are discussed in this article. Key challenges and research needs for developing adequate solutions are highlighted.

Introduction

The degradation of thermal-barrier coatings (TBCs) by molten deposits resulting from a combination of impurities introduced with the intake air and/or the fuel has been a concern since the introduction of these material systems in gas turbines. Corrosion by molten salts, especially alkaline sulfate-vanadate mixtures, was of early interest owing to (1) their potential for de-stabilization of the non-transformable, metastable tetragonal yttria-stabilized zirconia (*t'*-YSZ)[1–3] commonly used as a topcoat material and (2) their possible infiltration toward the thermally grown oxide (TGO) because their melting point is below the temperature of the TGO/TBC interface (see the Introductory article in this issue for a more detailed description of TBC structure). The latter could have two consequences, one related to a chemical attack of the TGO/bond coat,[4] and the other associated with freezing of the salt within the TBC on cooling and the ensuing loss of strain tolerance.[5] Phenomenological models have been developed to assess the effects of sulfate infiltration on coating life,[6] and promising materials solutions have been proposed.[7–9] However, currently adopted solutions rely primarily on fuel quality control.

As noted elsewhere in this issue, coatings are now enabling to the design of advanced gas turbines, whether based on metallic or ceramic components, with current goals calling for material surface temperatures ≥1500°C.[10] While low melting temperature salts remain a problem in some TBC applications, they do not constitute a fundamental barrier to increased performance, because the projected elevation in gas temperature would be above the dew point of most sulfate/vanadate salts. In contrast, the severe threat of silicate deposits at higher temperature operation was recognized quite early.[11–13] The problem arises from the ingestion of siliceous debris (airborne dust, sand, ash) that adheres to the surfaces in the hot gas path (combustors, airfoils, shrouds) and at peak temperatures of the engine cycle (e.g., take-off or landing) yields glassy melts based on calcium-magnesium alumino-silicates (CMAS). The glass wets all coating materials of interest and can (1) penetrate the TBC void spaces that accommodate the strain incompatibility with the metallic substrate and/or (2) chemically dissolve the coating material, usually followed by precipitation of a modified oxide.[12–16] Because all prospective TBCs have to be porous/segmented to render them strain-tolerant and most silicate deposits melt around 1200°C,[12,13,17,18] any increases in operating temperature needed to enhance turbine efficiency would require finding solutions to the CMAS problem. These deposits and the associated degradation of TBCs are therefore the primary focus of this article.

This article is organized into three main sections. The first section discusses the thermomechanical problem and the associated driving forces. The second addresses thermochemical

Carlos G. Levi, Materials Department, University of California, Santa Barbara; levic@engineering.ucsb.edu
John W. Hutchinson, School of Engineering and Applied Sciences, Harvard University; Hutchinson@husm.harvard.edu
Marie-Hélène Vidal-Sétif, Department of Metallic Materials and Structures, Onera, French Aerospace Lab; marie-helene.vidal-setif@onera.fr
Curtis A. Johnson, GE Global Research Center for Thermal Spray Research, Stony Brook University; johnsonca@nycap.rr.com
DOI: 10.1557/mrs.2012.230

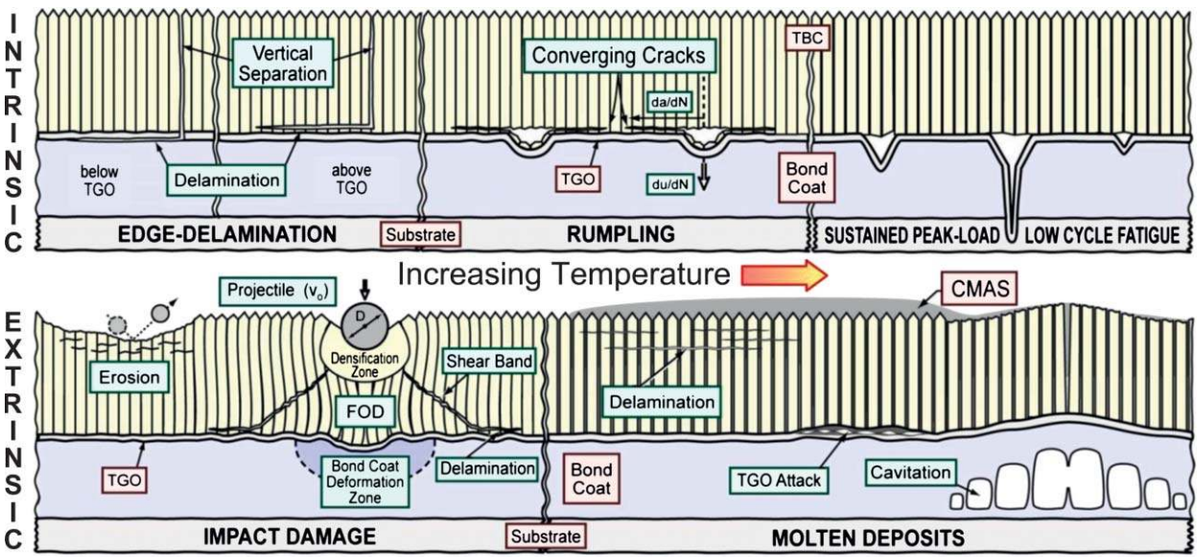

Figure 1. Extended menu of failure mechanisms typical of current thermal-barrier coatings (TBCs).[19] Three general modes of CMAS damage (lower right), characteristic of higher temperature operation, have been identified so far. One involves delamination cracks propagating through the TBC, another leads to chemical attack of the thermally grown oxide (TGO) with concomitant loss of adherence, and a third results from creep cavitation of the bond coat below a heavily penetrated TBC. FOD, foreign object damage; da/dN, crack growth per cycle; du/dN, inward displacement of TGO per cycle.

issues, which lead to opportunities for mitigation. The third deals with the experimental evaluation of the mitigation approaches. It finishes with a brief outlook on critical research needs.

Thermomechanical aspects

CMAS related damage mechanisms and field evidence

The TBC failure mechanisms identified to date are illustrated in **Figure 1**. While the role of CMAS is viewed primarily in terms of stiffening of the top *t'*-YSZ coat leading to shallow or deep delaminations,[13,20,21] recent work has shown that CMAS contact with the TGO results in chemical interactions and subsequent delamination along the TGO[22] or may promote creep cavitation in the bond coat wherein the delamination crack path would propagate within the metal, rather than the ceramic layers.[23] As turbine temperatures continue to increase, existing mechanisms will be aggravated, and new forms of damage may arise. Moreover, CMAS infiltration leads not only to stiffening of the coating, but also to degradation of the insulating properties of the TBC,[24,25] which may aggravate other intrinsic but nominally unrelated forms of degradation (e.g., rumpling[26]). The challenge of coating life prediction thus acquires new dimensions in the presence of CMAS.

An example of CMAS damage on current airfoils is depicted in **Figure 2** (left side) corresponding to state-of-the-art *t'*-YSZ TBCs in a commercial aircraft engine. While the thermal history cannot be ascertained, it is known that the engine operated short flights (i.e., frequent cycles with substantial hot periods) in dusty environments.[27] The distress is quite evident, extending beyond TBC loss to affect the TGO and bond coat, in some places exposing the base metal. (The coating on the right side of Figure 2 is discussed later in the text.)

Delamination damage due to CMAS has been studied in both commercial and military aircraft engines and exhibits common features in coatings produced by electron-beam physical vapor deposition (EBPVD)[20] as well as dense, vertically cracked TBCs produced by atmospheric plasma spray (APS).[21] In areas where the coating was cracked but not yet lost, the level

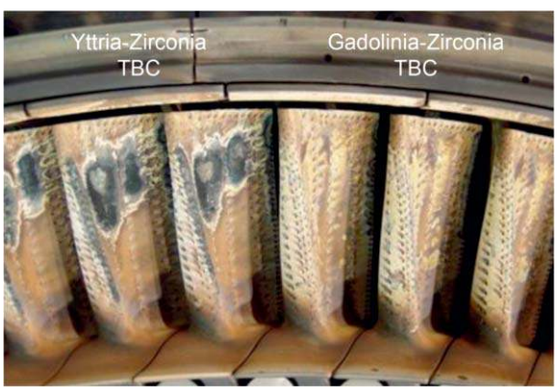

Figure 2. Comparison of typical distress experienced by conventional thermal-barrier coatings (TBCs) based on 7–8% yttria-stabilized zirconia with an advanced TBC based on $Gd_xZr_{1-x}O_{2-x/2}$ pyrochlore, where $x \approx 0.5$. The airfoils were part of an engine test in actual aircraft operation.[26] Courtesy of M.J. Maloney, Pratt & Whitney.

of CMAS penetration was about one-half of the total thickness, but deeper penetrations have been found in other airfoils. The driving forces behind these failures are now examined briefly.

Understanding the driving force for thermo-mechanical failure

Release of the elastic strain energy stored in the coating supplies the underlying driving force for the delamination and spalling of TBC coatings.[28] The major source of this elastic energy is the thermal expansion mismatch between the coating and the metal substrate that occurs upon cooling. To facilitate understanding of the origin of this elastic energy, the following discussion will focus first on isothermal cooling of the TBC/substrate system and then consider more representative scenarios involving a thermal gradient through the system in the hot state and transient cooling.

Stress in the coatings is relaxed by creep at high temperatures, and, thus, a reasonable working assumption is that the coating stresses are zero at the hottest operating state. Cool-down is relatively rapid, such that in most instances, one may assume that thermoelastic behavior applies with no further creep relaxation. Clear insights into the coating stress and elastic energy emerge from a model that views the substrate as thick and at uniform temperature.[28] The substrate constrains bending, which is taken to vanish in the model and imposes an in-plane biaxial strain change, $-\alpha_s \Delta T_{sub}$, on the coating. Here, α_s is the thermal expansion coefficient of the substrate and, during cooling, $\Delta T_{sub} = T^0_{sub} - T_{sub}$ is the temperature drop of the substrate from its temperature in the hot state, T^0_{sub}. For simplicity, the coefficients of thermal expansion will be taken to be temperature-independent. In the hot state, a steady-state temperature distribution exists with T^0_{sur} at the coating surface and T^0_{sub} at its interface with the substrate. The temperature drop of the coating surface relative to the substrate is denoted by $\Delta T_{sur/sub} = \left(T^0_{sur} - T_{sur}\right) - \Delta T_{sub}$.

Consider a single layer uniform coating with Young's modulus, E_c, Poisson's ratio, ν_c, coefficient of thermal expansion, α_c, and thickness, h_c. At any stage during cool-down, idealize the temperature distribution in the coating to be linear according to

$$\Delta T(y) = \Delta T_{sub} + (y/h_C)\Delta T_{sur/sub}, \quad (1)$$

with y as the through-thickness coordinate measured from the interface. At any stage during cool-down, the state of stress in the layer is equibiaxial, in-plane, given by

$$\sigma(y) = \frac{E_C}{1-\nu_C}\left(-\Delta\alpha_C \Delta T_{sub} + (y/h_C)\alpha_C \Delta T_{sur/sub}\right). \quad (2)$$

This equation reveals that cooling of the coating relative to the substrate generates tensile stress depending on the full coefficient of thermal expansion of the coating, while cooling of the substrate imposes stress on the coating depending on the thermal expansion mismatch, $\Delta\alpha_c = \alpha_S - \alpha_c$. The elastic energy per area in the coating associated with these thermal stresses, available for release of the coating from the substrate under plane strain conditions, is

$$U = \frac{E_C h_C (1+\nu_C)}{2(1-\nu_C)}\left\{(\Delta\alpha_C \Delta T_{sub})^2 - (\Delta\alpha_C \Delta T_{sub})(\alpha_C \Delta T_{sur/sub}) + \frac{1}{3}(\alpha_C \Delta T_{sur/sub})^2\right\}. \quad (3)$$

The interaction term, $(\Delta\alpha_C \Delta T_{sub})(\alpha_C \Delta T_{sur/sub})$, is important, and it arises because the compressive coating stress driven by cooling of the substrate, ΔT_{sub}, can be offset by the tensile stress associated with cooling of the coating surface relative to the substrate, $\Delta T_{sur/sub}$. For the calculations shown here, $\alpha_C = 11 \times 10^{-6}\ C^{-1}$, $\alpha_S = 13 \times 10^{-6}\ C^{-1}$, and the coating's Poisson's ratio is $\nu_c = 0.2$.

The elastic energy/unit area given by Equation 3 is plotted in normalized form ($U/E_c h_c$) in **Figure 3**. Two limiting scenarios are insightful. The first applies when the coating and substrate have a uniform temperature both in the hot state and while cooled (i.e., ΔT_{sub} increases while $\Delta T_{sur/sub} = 0$). This is representative of furnace cycle tests involving isothermal holds and relatively slow-cooling. Given that U scales with h_c and considering a typical in-plane modulus absent CMAS penetration, $E_c = 30$ GPa, a "thin" 200 μm TBC illustrative of aero-engine blades would build up an elastic energy of ~11 J·m^{-2} on cooling from $T^0_{sub} = 800$°C, whereas a "thick" 1-mm coating that might be found in power generation components would reach ~58 J·m^{-2} under the same conditions. Whether failure would occur depends, of course, on the coating toughness under the pertinent crack propagation mode, which is not well characterized for these systems.

Consider now the case where the TBC is stiffened by complete penetration of CMAS, elevating the Young's modulus to at least that of typical glasses (i.e., $E_c = 90$ GPa). (Higher values are likely given that most of the coating is dense *t'*-YSZ, with $E_{YSZ} \approx 200$ GPa.) The elastic energy accumulated in the same thermal excursion for the representative "thin" and "thick" coatings cited previously would then go up by a factor of 3, to ~35 and ~173 J·m^{-2}, respectively. This simple result gives the clearest insight into the role CMAS plays in debilitating a TBC by degrading its in-plane compliance. CMAS infiltration also alters other properties of the coating such as the coefficient of thermal expansion and the thermal conductivity,[24,25] but from the vantage point of delamination, the major effect is the boost in the coating modulus. While CMAS seldom infiltrates all the way to the coating/substrate interface, as assumed in computing Figure 3 with a single value of E_c, its effect on the elastic energy in the coating is self-evident. In particular, a coating with an ample reserve against delamination may experience a factor-of-two increase in elastic energy/area due to thermal stresses when partially infiltrated by CMAS.[21,28]

The second scenario of interest in Figure 3 is one wherein the substrate temperature remains relatively unaffected, $\Delta T_{sub} \approx 0$, but the coating surface temperature drops rapidly relative to the substrate, $\Delta T_{sur/sub} > 0$. This may occur, for example, if cool

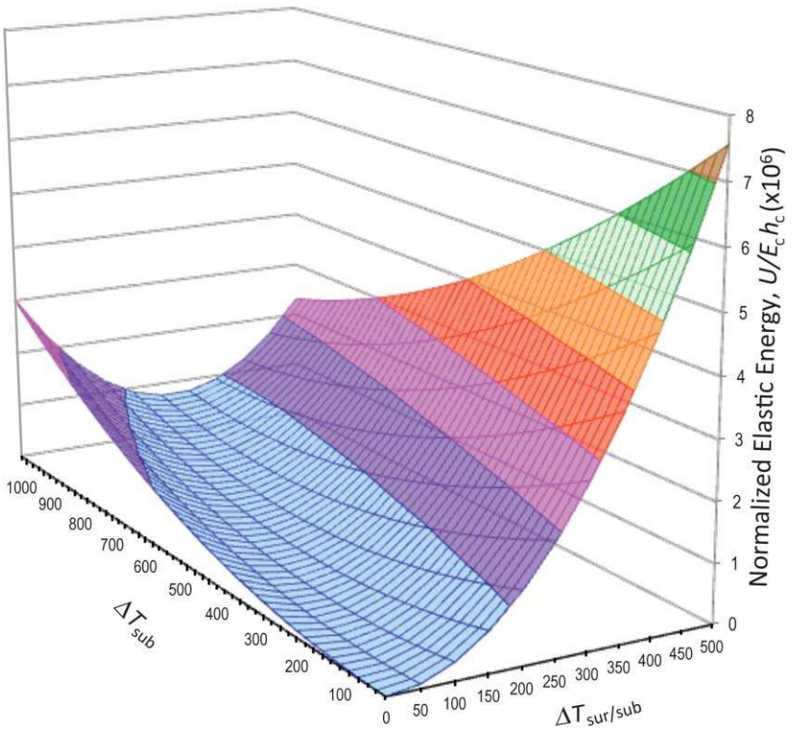

Figure 3. Normalized elastic energy/area in the coating (U/E_ch_c) calculated from Equation 3 and available for release under plane strain conditions due to thermal stress induced by cooling from an initially high temperature. ΔT_{sub} and $\Delta T_{sur/sub}$ are the temperature drops of the substrate and of the coating surface relative to the substrate, respectively, and the properties of the coating/substrate system are as defined in the text. Note that any value of U would scale with the coating modulus E_c (e.g., due to stiffening by calcium-magnesium alumino-silicate penetration) and with the coating thickness, h_c. Also note that cooling paths wherein $\Delta T_{sur/sub}$ and ΔT_{sub} change simultaneously may result in much lower strain energy buildup.

gas suddenly impinges on the coating owing to an unexpected flameout of an engine. As seen in Equation 2, the thermal stress in the coating is now proportional to $\alpha_c\Delta T_{sur/sub}$, and it develops primarily from self-constraint of the coating to thermal contraction as its surface cools faster than the region closer to the substrate. The trend in elastic energy/area that arises from this contribution corresponds to the trace of the U/E_ch_c surface in Figure 3 with the plane $\Delta T_{sub} \approx 0$. If a rapid cooling event occurs with $\Delta T_{sur/sub}$ as large as 400°C, the elastic energy in the coating in the early stage of cool-down could exceed that at the final cool-down (cf. the "quench" scenario in Figure 8c). It is also evident from Figure 3 that the buildup of elastic energy can be ameliorated when both ΔT_{sub} and $\Delta T_{sur/sub}$ define a path along the valley in the U/E_ch_c surface (cf. the "slow cool" scenario in Figure 8c).

Numerous thermal scenarios beyond those presented previously must be considered to assess the ability of a TBC to resist delamination.[29] To set the foundation for the discussion of thermal gradient tests (see the section on Assessing the mitigation strategy), a rapid cooling scenario will be illustrated for a system having a superalloy substrate 3.5 mm thick coated by a representative *t'*-YSZ layer with $h_c = 1$ mm. The initial steady-state temperatures of the coating surface and the underside of the substrate are $T^0_{sur} = 1300$°C (above the melting point of most typical CMAS deposits) and 800°C, respectively, with $T^0_{sub} = 830$°C at the coating/substrate interface. Starting at time $t = 0$, forced cooling air at 35°C is switched on, impinging on the coating surface, with nominally stagnant air at 35°C on the underside of the substrate. (This would not be typical of engine operation but is of interest in laboratory tests.) The transient temperature history shown in **Figure 4**a has been computed using heat transfer coefficients representative of forced air cooling at the coating surface and radiative cooling with natural convection at the underside.[29] In this figure, ΔT_{sub} is identified with the temperature drop at the interface, and $\Delta T_{sur/sub}$ is the temperature drop of the coating surface relative to that at the interface. Within the first several seconds, $\Delta T_{sur/sub}$ peaks at ~650°C, while ΔT_{sub} remains relatively small. As the cooling progresses, the approach to the asymptotic limits in Figure 4a reflect cooling of the substrate to room temperature and the contribution of the initial temperature gradient across the coating to $\Delta T_{sur/sub}$.

Transient histories of elastic energy/area in the coating, U, based on the transient temperature drops in Figure 4a, are plotted in Figure 4b for a uniform coating 1 mm thick and for a 1 mm coating having an upper layer of thickness 0.25 mm penetrated by CMAS. α_c, α_c, and ν_c are as specified. The lower curve for the uniform coating with no CMAS was computed using Equation 3. The upper curve was computed with an equation similar to 3, but more complicated, for a bilayer coating. For simplicity, the CMAS layer was assumed to have solidified as soon as cooling commenced, with the coating surface at 1300°C. In addition, only E_c was assumed to have been altered by CMAS; the thermal properties are assumed to remain the same as those of the unpenetrated coating.

The evolution of U in Figure 4b reveals that a TBC will experience a peak in elastic energy in the early stage of a rapid cool-down, within about 2 s for a 1 mm thick coating. More importantly, CMAS penetration in the upper quarter of the coating would double this peak energy. In the presence of an initial thermal gradient, the 1 mm coating is most susceptible to delamination under rapid cooling when the elastic energy due to the thermal stress peaks. Under this scenario, the energy/area in the cold state is much less than the early stage peak. This is partly due to the fact that the tensile stress in the cold state, due to the initial temperature gradient contribution to $\Delta T_{sur/sub}$, is offset by the compressive stress induced by the thermal expansion mismatch with the substrate.

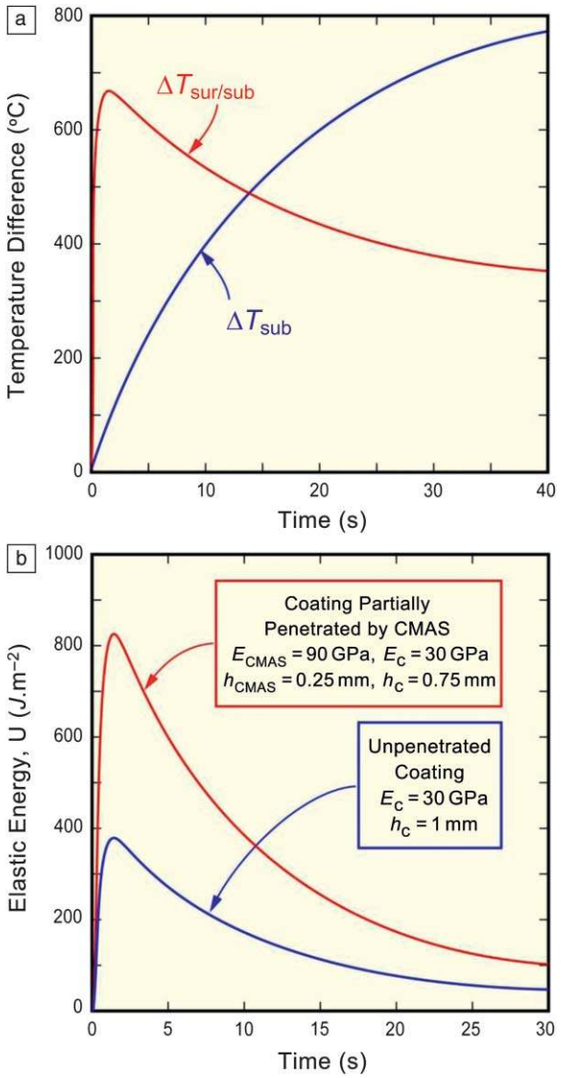

Figure 4. Transient temperature drops of the substrate (ΔT_{sub}) and of the coating surface relative to the substrate interface ($\Delta T_{sur/sub}$) (a) and associated transient elastic energy/area of the coating (b) for a sudden cooling event in which ambient air (35°C) impinging on the surface of the coating is switched on at $t = 0$. $T^0_{sur} = 1300$°C and $T^0_{sub} = 830$°C.

Coating design for resistance to delamination requires analysis of other thermal scenarios with due consideration given to the role of CMAS, as evident from the earlier discussion. A simplified model has been used here to reveal trends. More accurate calculations are required to account for details such as the full temperature distribution, bending of the substrate, and the crystallization/glass-transition temperature of the CMAS. Moreover, the energy release rate and mode mix associated with delamination cracking can be computed accurately with enhanced models. The trends for the energy release rate follow those for the stored elastic energy/area, *U,* quite closely.

Thermochemical aspects

Notwithstanding the predominantly thermomechanical origin of the CMAS-related TBC failures, substantial effort has been invested toward understanding the thermochemical interactions with *t'*-YSZ (e.g.,[12–14,26,30–33]). However, *t'*-YSZ is unlikely to meet the long-term requirements for advanced engines even when CMAS is not a concern, because of inherent limitations in its phase stability above ~1200°C.[34–36] Conversely, understanding the chemical interactions is essential for developing alternate coatings, since CMAS nominally attacks all oxides of interest for thermal (and environmental) barriers. Materials that may outperform *t'*-YSZ in a CMAS environment already exist, as illustrated in Figure 2,[37] but with penalties in critical properties such as toughness (see the Pan et al. article in this issue).[38] This section briefly addresses the salient issues regarding the nature of the deposits, the lessons learned from *t'*-YSZ, and the experiences with proposed mitigation strategies.

Sources and composition of silicate deposits

A key challenge in understanding thermochemical interactions and developing a foundation for life prediction models is the uncertainty in the amount and chemical composition of the molten glass formed on the coating surface. In general, compositions of actual engine deposits are significantly different from the common sources of siliceous minerals (**Figure 5**). The rationale is that only the finer particles (<10 μm) ingested with the intake air contribute to the deposit buildup.[17,39] Moreover, the deposits contain oxides originating from the engine components, presumably by erosion (e.g., NiO, TiO_2, ZrO_2).[13,26] It has also been shown that the composition of melts infiltrating the TBC are not necessarily the same as those of the deposits, suggesting partial melting of the latter. The infiltrated CMAS were reported to have similar compositions for a wide variety of deposits, loadings, and severity of exposure.[13] However, the diversity of reaction products with the *t'*-YSZ, discussed later, suggests that the CMAS compositions may vary more widely than originally suggested.

The mechanism and rate of deposit buildup remain under debate. One might anticipate that the siliceous "dust" melts in flight through the combustor and deposits as droplets. Examination of some airfoil deposits, however, reveals agglomerates of solid particulates, implying that melting might occur *in situ*, probably during the hotter stages of the engine cycle, but the details are obscure. The rate of accumulation also varies over the surface of an airfoil, concentrating on the hotter areas of the higher pressure side and, to some extent, on the leading edge, with little or no deposits on the suction side.[26,33,39]

Experiences with t'-YSZ

The primary mechanism of interaction between a molten silicate glass and an oxide is that of dissolution and, upon saturation, re-precipitation of one or more crystalline phases closer to equilibrium with the melt,[14] cf. **Figure 6**. When penetration is extensive, as in *t'*-YSZ under isothermal exposure above the CMAS melting point (cf. Figure 7 in the Introductory article),

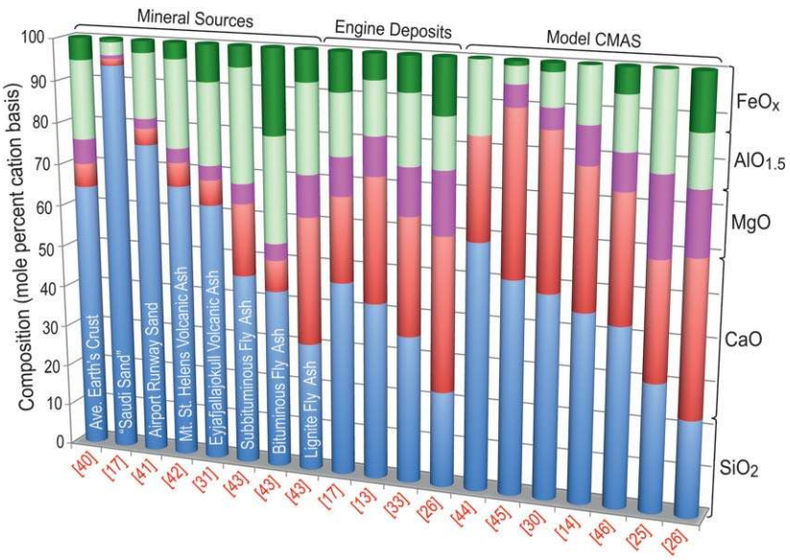

Figure 5. Concentration of predominant oxides in the composition of calcium-magnesium alumino-silicates, grouped by examples of sources of siliceous debris, compositions reported for actual deposits in engines, and model compositions used in laboratory investigations of the problem. (Small additions in some model compositions are not included.) Within each group, the compositions are listed from left to right in order of descending SiO_2 content, except for the average composition of the earth's crust that serves as a reference. Reference citations are listed along the bottom of the image.

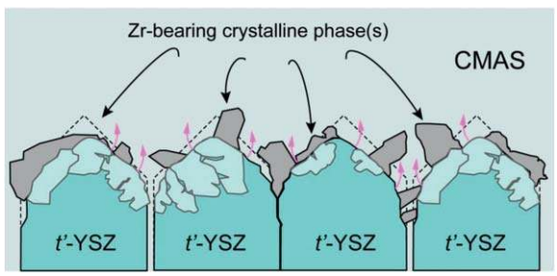

Figure 6. Schematic illustration of the dissolution-reprecipitation mechanism in yttria-stabilized zirconia, wherein the coating material dissolves in the molten glass and reprecipitates as one or more compositionally modified crystalline phases. Some of the phases may form at high temperature, whereas others may precipitate upon cooling.

the extent of interaction can be significantly different within the pore spaces, where the melt volume is small relative to the TBC, compared with the surface, where the relative proportion of melt is much larger. Laboratory approaches aiming to replicate the interaction in service range from those using materials sampled from the field,[12,13,31] to the use of "synthetic CMAS" similar in composition to the deposit (see References 32 and 47), to studies using simplified compositions with only a few oxides.[14,44,49]

In a baseline study, *t'*-YSZ (EBPVD) dissolved isothermally in a model CMAS melt with (Ca+Mg):Si ≈ 0.93 (1300°C/4h) and reprecipitated either Y-lean ZrO_2, transformable to monoclinic on cooling, or fully stabilized Y-rich cubic ZrO_2, depending on the alumina content of the melt.[14] Similar observations were made on APS *t'*-YSZ exposed to a more complex CMAS with (Ca+Mg):Si ≈ 0.86 (1121°C/24h).[30] In contrast, a simpler CAS melt with Ca:Si ≈ 0.41 and similar Al (1200°C/4h) yielded $Ca_2ZrSi_4O_{12}$.[49] A complex "synthetic volcanic ash" with an even lower (Ca+Mg):Si ≈ 0.15 (1200°C/1h) was reported to form $ZrSiO_4$ (zircon) at the interface, whereas a lignite fly ash with a much higher (Ca+Mg):Si ≈ 1.1 produced predominantly tetragonal YSZ.[31] In most of these experiments, the residual CMAS was largely amorphous upon cooling, although crystalline silicates were found in some cases. Observations in field specimens were at least qualitatively consistent with these simulated exposures, with no evidence that the reaction products played a significant role in mitigating penetration and the ensuing stiffening. In one peculiar service airfoil, where $CaSO_4$ was found to have infiltrated the TBC prior to CMAS exposure, there was no detectable reaction within the spaces in the columnar *t'*-YSZ structure, but $CaZrO_3$ was found on top of the column tips.[26] The latter reacted with the overlying silicate melt, presumably deposited later, to yield a complex garnet phase (kimzeyite) with composition $Ca_3(Zr,Mg,Ti)_2(Fe,Al,Si)_3O_{12}$. One might speculate that this reaction layer has potential for CMAS mitigation, but at the expense of infiltrating the TBC with solid $CaSO_4$, which would compromise the strain tolerance of the coating. While the coating survived in this case, this does not appear to be a practical solution in the long term.

Mitigation strategies

Numerous CMAS mitigation strategies for YSZ have been proposed in the literature,[46,50,51] but the persistence of the problem suggests they have not been as effective as expected. Most current approaches are based on manipulating the chemical reaction between the TBC and the melt to accomplish two goals simultaneously: (1) "immobilize" the melt by capturing its main constituents into crystalline phases, most obviously silicates, and (2) generating enough volume of precipitated products to fill the pore spaces and block access of any residual melt to the remaining TBC. The implications are that (1) the chemical reaction should yield stable crystalline products in excess of the simple reprecipitation of the Zr-rich phases, since those are essentially replacing the dissolved material, and (2) the kinetics of both the dissolution and reprecipitation processes must be competitive with the infiltration kinetics (i.e., the reaction must be quite fast).

Two broad strategies based on reactivity can be distinguished. One is based on alumina as the key reactant, which combines with CaO and SiO_2 to form anorthite, $CaAl_2Si_2O_8$. The seemingly most successful approach in this category involves the incorporation of alumina in metastable solid solution in

YSZ, with a small amount of TiO_2 to catalyze the crystallization process.[30,47] Because the volume of alumina required for effective mitigation is well beyond its equilibrium solubility in ZrO_2, the approach exploits the ability of solution precursor plasma spray[52] to generate the desired coatings (see the Sampath et al. article in this issue for a description of this technique).

The second mitigation strategy is based on rare-earth (RE) zirconates, exemplified by $Gd_2Zr_2O_7$ (GZO).[31,53,54] This is the material showing no significant distress on the right-hand side of Figure 2. The merit of the approach relies on the dissolution of $RE_2Zr_2O_7$ to precipitate a $Zr(RE,Ca)O_x$ fluorite phase combined with a highly stable apatite silicate with nominal composition $Ca_2RE_8(SiO_4)_6O_2$, where RE can be Y or one of the lanthanides from La to Yb.[54] The mechanism is illustrated in **Figure 7** and proceeds as follows: (a) the glass melt rapidly wets the inner surfaces of the columns, with some features of the interaction suggesting intriguing topography effects on melt spreading; (b) re-precipitation of fluorite starts soon thereafter, concurrent with that of apatite (faceted crystals) in the narrower spaces, indicating that dissolution was already occurring at the shortest time; (c) generalized precipitation of apatite and fluorite, filling first the narrower gaps wherein supersaturation is achieved earlier; (d) gaps are sealed, and the column surface is covered with a nominally dense layer of reaction product, which acts as a diffusion barrier; and (e) after the gaps are sealed (reflected in the ghost structures projecting from the voided column gaps underneath), reaction continues at a much slower rate consuming the column tips. The CMAS used in these experiments had Ca:Si ≈ 0.73, whereas the apatite product has Ca:Si = 0.33, implying that the melt should be preferentially depleted in Si upon reaction, with concomitant reduction in melt volume. Recent experiments have shown that similarly favorable reactions take place with other zirconates.[44,48]

To the best of the authors' knowledge, Gd-zirconate has now been in operation in engines for several years after the successful experience depicted in Figure 2. RE zirconates generally offer lower thermal conductivity and enhanced sintering resistance relative to *t'*-YSZ, although some concerns remain about their lower toughness.[55] Alternate compositions, including those based on other zirconates, as well as on alumina+titania additions, remain under investigation.

Assessing the mitigation strategy

Developing and optimizing a mitigation strategy requires insight into two major topics, namely the comparative kinetics of the infiltration, dissolution, and reprecipitation processes, and the mechanical robustness of the stiffened layers generated by the CMAS/TBC reactions. Thermal analysis coupled with microstructural observations can be used to assess the activity of the reaction.[57] Notably, recent measurements on the ZrO_2-Nd_2O_3 system[44] have determined that the dissolution rate of the oxide depends on the RE concentration, confirming that the pyrochlore structure zirconate not only promotes the precipitation of apatite, but also the rapid dissolution of the TBC, both needed to compete with the infiltration kinetics. It is also worth noting the potential effects of the initial state of the CMAS reactant. Pre-melted amorphous CMAS has homogeneity advantages but also leads to uncertainty in the behavior upon heating, since some compositions crystallize

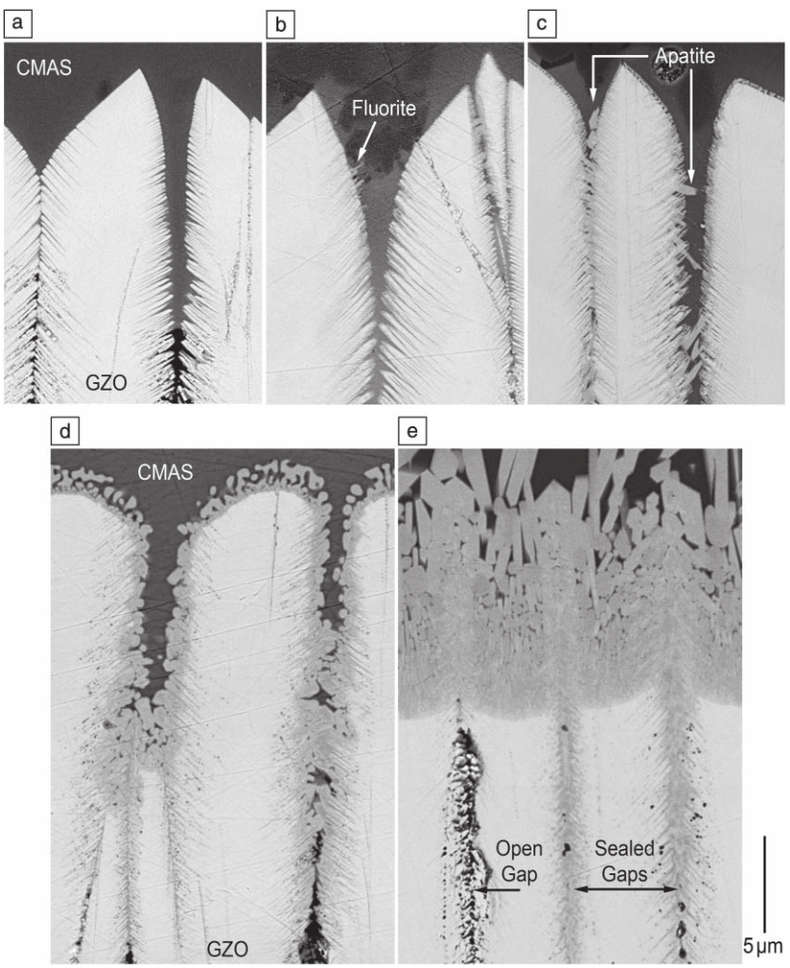

Figure 7. Illustration of the sequence of events that leads to the sealing of the intercolumnar gaps owing to the chemical interaction of calcium-magnesium aluminosilicates (CMAS) with a Gd zirconate electron beam physical vapor deposition coating (see the Introductory article of this issue). The top images represent the early stages of the reaction and were generated using amorphous CMAS heated rapidly to 1150°C for (a) 10s, (b) 20s, and (c) 30s. The bottom specimens were longer time exposures using initially crystalline CMAS (d) 4 min above the melting point and immediately cooled down, and (e) 4h at 1300°C. Images courtesy of S. Krämer.

and then melt, whereas others soften gradually, complicating the interpretation of the heat evolution history.[57]

Thermomechanical assessment of CMAS infiltrated/reacted systems is still in its infancy. Thermal gradient tests are essential since "isothermal" furnace cycle tests can lead to misleading results, and tests at 1300°C and above would compromise superalloy substrates. Jet engine thermal shock (JETS) tests[50,56] are often used to assess the performance of TBCs under thermal gradients and have been extended to CMAS testing (see the Vaβen et al. article in this issue). Burner rigs have also been modified to enable the injection of CMAS precursor solutions through the flame[45] and are used successfully for testing plasma spray $ZrYAlTiO_x$ coatings.[58] In both cases, the temperatures in the front and back of the specimen are measured during the cycle and used to calculate the evolution of the strain energy.[28] A thermal gradient test based on a laser heat source, schematically depicted in **Figure 8**a, has been recently developed.[59] Proper specimen design allows monitoring of not only the temperature at the surface and the backside of the substrate, but also near the TGO/TBC interface. Thermal histories can be accurately recorded and carefully manipulated using the laser power-up and -down rates (e.g., Figure 8b). In addition, the system is set up with blue LED illumination and suitable filters,[60] allowing visual monitoring of the coating surface during heating and cooling. The thermal history can then be cast in terms of ΔT_{sub} and $\Delta T_{sur/sub}$ (as discussed in the section on Understanding the driving force for thermomechanical failure), and used to calculate the strain energy buildup during cooling, Figure 8c. Specimens are then examined after testing to identify the type and extent of damage, Figure 8d–e, which can in turn be correlated to the thermal history. It is anticipated that this instrument will be invaluable in testing materials systems and in helping refine the models needed to build life prediction capabilities for TBCs with CMAS.

Outlook

The CMAS problem in thermal-barrier coatings (TBCs) is intrinsically thermomechanical, but thermochemical issues are relevant to formulating an effective mitigation strategy. Because the driving force for delamination scales with the square of the temperature drop, the problem is expected to increase in severity as TBCs are pushed to higher surface temperatures, while the TBC/thermally grown oxide interface remains near present levels. The grand challenge of the field is the search for a viable oxide that offers both CMAS resistance and adequate toughness. For zirconia/hafnia based systems, the challenge arises from the dichotomy in design approaches *viz*, CMAS resistant compositions require large concentrations of reactive dopants [Y, RE, Al], whereas tough compositions are based on tetragonal crystal structures with much lower dopant content.

Developing the science base to guide the materials development effort requires the effective integration of modeling and

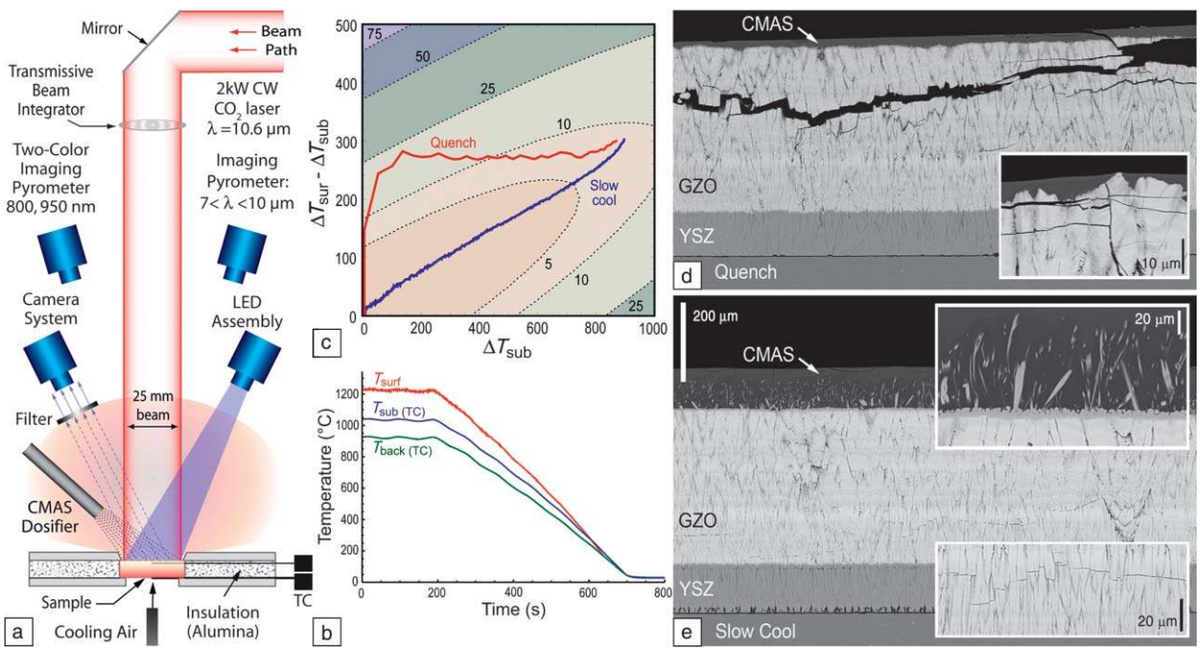

Figure 8. Illustration of a (a) thermal gradient test based on a continuous CO_2 laser with backside cooling and extensive instrumentation used to probe the response of coatings infiltrated with calcium-magnesium alumino-silicates to various thermal excursions. The thermal histories (e.g., (b)) can be varied over a substantial range, and ensuing thermal stresses and associated strain energies can be estimated based on models such as those described in the text; (c) projection of the surface in Figure 3 where the contours represent different levels of elastic energy and the paths are two representative thermal excursions corresponding to the samples whose micrographs are illustrated in (d) and (e). The insets show details of the cracks and in (e) the layer of reaction products on the surface of the GZO. Images courtesy of R.W. Jackson.

experimental activities, ideally under an integrated computational materials engineering (ICME) framework.[61] There is a paucity of thermodynamic information on the relevant multicomponent systems to help identify promising compositions that may enable both improvements in toughness and effective reactivity with CMAS melts, as well as to evaluate the sensitivity of candidate materials to the expected variability in melt compositions. Improvements are also needed in the modeling outlined in this article for predicting delamination driving forces, including, for example, assessment of the extent of stress relaxation at the highest temperatures and during cool-down and the interplay of multilayer architectures. Studies on the relevant infiltration, dissolution, and crystallization kinetics for the appropriate combinations of silicate melts and thermal barrier oxides are also essential. Once desirable compositions are identified, it would be necessary to develop the processing science to enable their optimal synthesis into coatings.

On the experimental side, there is a long-standing need for adequate methods for measuring and characterizing the mechanical and thermal properties of coatings at high temperatures, including microstructures produced by thermochemical interactions. It is worth noting that it has been a significant challenge for the field to devise methods to measure delamination toughness, yet this is crucial in developing design approaches to TBCs. Only within the past few years have experimental methods emerged that are capable of measuring coating and interface toughness with reasonable accuracy, but only at temperatures close to ambient. The challenges are daunting, but so are the needs for improving materials that would enable more efficient gas turbines for energy and propulsion.

Acknowledgments

This article draws on lessons from research supported by the Office of Naval Research (CGL) and the French Defense Research Organization (MHVS). The authors are indebted to Dr. M.J. Maloney (PWA) for use of the illustration in Figure 2, as well as to Drs. O. Lavigne (ONERA), D. Konitzer, and D. Lipkin (GE) and Professors N.P. Padture (Brown) and M.R. Begley (UCSB) for helpful discussions. The contributions of Drs. R.W. Jackson and S. Krämer at UCSB are gratefully acknowledged.

References

1. D.W. McKee, P.A. Siemers, *Thin Solid Films* **73**, 439 (1980).
2. A.S. Nagelberg, *J. Electrochem. Soc.* **132** (10), 2502 (1985).
3. R.L. Jones, C.E. Williams, *Surf. Coat. Technol.* 349 (1987).
4. C. Leyens, I.G. Wright, B.A. Pint, *Oxid. Met.* **54** (5/6), 401 (2000).
5. T.E. Strangman, *Thin Solid Films* **127**, 93 (1985).
6. T.E. Strangman, J. Neumann, A. Liu, "Thermal Barrier Coating Life—Prediction Model Development; Final Report" (NASA–Lewis Research Center, 1987).
7. R.L. Jones, "Experiences in Seeking Stabilizers for Zirconia having Hot Corrosion-Resistance and High Temperature Tetragonal (t') Stability" (NRL/MR/6170–96–7841, Naval Research Laboratory, 1996).
8. S. Raghavan, M.J. Mayo, *Surf. Coat. Technol.* **160**, 187 (2002).
9. F.M. Pitek, C.G. Levi, *Surf. Coat. Technol.* **201**, 6044 (2007).
10. M.A. Alvin, F.S. Pettit, G.H. Meier, N.M. Yanar, M. Chyu, D. Mazzotta, W. Slaughter, V. Karaivanov, B. Kang, C. Feng, R. Chen, T.C. Fu, in *5th International Conference on Advances in Materials Technology for Fossil Power Plants*, R. Viswanathan, D. Gandy, K. Coleman, Eds. (Electric Power Research Institute, Inc., Marco Island, FL, 2008), pp. 413–423.
11. J.L. Smialek, F.A. Archer, R.G. Garlick, *JOM* **46** (12), 39 (1994).
12. F.H. Stott, D.J. de Wet, R. Taylor, *MRS Bull.* **19** (10), 46 (1994).
13. M.P. Borom, C.A. Johnson, L.A. Peluso, *Surf. Coat. Technol.* **86–87**, 116 (1996).
14. S. Krämer, J.Y. Yang, C.A. Johnson, C.G. Levi, *J. Am. Ceram. Soc.* **89** (10), 3167 (2006).
15. K.M. Grant, S. Krämer, J.P.A. Löfvader, C.G. Levi, *Surf. Coat. Technol.* **202**, 653 (2007).
16. K.M. Grant, S. Krämer, G.G.E. Seward, C.G. Levi, *J. Am. Ceram. Soc.* **93** (10), 3504 (2010).
17. J.L. Smialek, "The Chemistry of Saudi Arabian Sand: A Deposition Problem on Helicopter Turbine Airfoils" (NASA TM-105234, NASA Lewis Research Center, 1991).
18. W. Braue, *J. Mater. Sci.* **44**, 1664 (2009).
19. A.G. Evans, D.R. Clarke, C.G. Levi, *J. Eur. Ceram. Soc.* **28** (7), 1405 (2008).
20. C. Mercer, S. Faulhaber, A.G. Evans, R. Darolia, *Acta Mater.* **53** (4), 1029 (2005).
21. S. Krämer, S. Faulhaber, M. Chambers, D.R. Clarke, C.G. Levi, J.W. Hutchinson, A.G. Evans, *Mater. Sci. Eng., A* **490**, 26 (2008).
22. V.K. Tolpygo, private communication.
23. K.M. Wessels, R.W. Jackson, D.G. Konitzer, T.M. Pollock, C.G. Levi, presented at the International Conference on Metallurgical Coatings and Thin Films, San Diego, CA, 2012.
24. L. Li, D.R. Clarke, *Int. J. Appl. Ceram. Technol.* **5** (3), 278 (2008).
25. J. Wu, H.B. Guo, Y.Z. Gao, S.K. Gong, *J. Eur. Ceram. Soc.* **31**, 1881 (2011).
26. W. Braue, P. Mechnich, *J. Am. Ceram. Soc.* **94** (12), 4483 (2011).
27. M.J. Maloney, in *Turbine Forum* (Forum of Technology, Germany, Nice-Port St. Laurent, France, 2006).
28. A.G. Evans, J.W. Hutchinson, *Surf. Coat. Technol.* **201**, 7905 (2007).
29. S. Sundaram, D.M. Lipkin, C.A. Johnson, J.W. Hutchinson, *J. Appl. Mech.* (2012), in press.
30. A. Aygun, A.L. Vasiliev, N.P. Padture, X. Ma, *Acta Mater.* **55** (20), 6734 (2007).
31. A.D. Gledhill, K.M. Reddy, J.M. Drexler, K. Shinoda, S. Sampath, N.P. Padture, *Mater. Sci. Eng., A* **528**, 7214 (2011).
32. P. Mechnich, W. Braue, U. Schulz, *J. Am. Ceram. Soc.* **94** (3), 925 (2011).
33. M.-P. Bacos, J.-M. Dorvaux, O. Lavigne, R. Mévrel, M. Poulain, C. Rio, M.-H. Vidal-Setif, in *Aerospace Lab: The ONERA Journal* (ONERA, Chatillon, France, 2011), issue 3.
34. R.A. Miller, J.L. Smialek, R.G. Garlick, in *Science and Technology of Zirconia*, A.H. Heuer, L.W. Hobbs, Eds. (The American Ceramic Society, Columbus, OH, 1981), vol. 3, pp. 241–253.
35. J.A. Krogstad, S. Krämer, D.M. Lipkin, C.A. Johnson, D.R.G. Mitchell, J.M. Cairney, C.G. Levi, *J. Am. Ceram. Soc.* **94** (S1), S168 (2011).
36. D.M. Lipkin, J.A. Krogstad, Y. Gao, C.A. Johnson, W.A. Nelson, C.G. Levi, *J. Am. Ceram. Soc.* (2012), in press.
37. M.J. Maloney, US Patent 6,177,200, 2001.
38. R. Vassen, A. Stuke, D. Stöver, *J. Therm. Spray Technol.* **18** (2), 181 (2009).
39. T.E. Strangman, D. Raybould, A. Jameel, W. Baker, *Surf. Coat. Technol.* **202**, 658 (2007).
40. W.E. Ford, in *Dana's Textbook of Mineralogy with an Extended Treatise on Crystallography and Physical Mineralogy, 4th Edition* (Wiley, New York, 1954).
41. PTI, "Material Safety Data Sheet: Airport Runway Sand" (2007); www.powdertechnologyinc.com/secondary/msds.php.
42. H.E. Taylor, F.E. Lichte, *Geophys. Res. Lett.* **7** (11), 949 (1980).
43. W. Chesner, R. Collins, M. MacKay, J. Emery, "User Guidelines for Waste and Byproduct Materials in Pavement Construction" (Federal Highway Administration, Washington, DC, 1997).
44. N. Chellah, M.-H. Vidal-Sétif, C. Petitjean, P.-J. Panteix, C. Rapin, M. Vilasi, in *8th International Symposium on High Temperature Corrosion and Protection of Materials (HTCPM8)* (Les Embiez, France, 2012).
45. T. Steinke, D. Sebold, D.E. Mack, R. Vaßen, D. Stöver, *Surf. Coat. Technol.* **205**, 2287 (2010).
46. A.K. Rai, R.S. Bhattacharya, D.E. Wolfe, T.J. Eden, *Int. J. Appl. Ceram. Technol.* **7** (5), 662 (2010).
47. J.M. Drexler, K. Shinoda, A.L. Ortiz, D. Li, A.L. Vasiliev, A.D. Gledhill, S. Sampath, N.P. Padture, *Acta Mater.* **58** 6835 (2010).
48. J.M. Drexler, A.L. Ortiz, N.P. Padture, *Acta Mater.* **60** 5437 (2012).
49. M.-P. Bacos, J.-M. Dorvaux, S. Landais, O. Lavigne, R. Mévrel, M. Poulain, C. Rio, M.-H. Vidal-Sétif, in *Aerospace Lab: The ONERA Journal* (ONERA, Chatillon, France, 2011), issue 3.
50. W.C. Hasz, C.A. Johnson, M.P. Borom, US Patent 5,660,885 (1997).

51. M. Fu, R. Darolia, M.D. Gorman, B.A. Nagaraj, US Patent 8,062,759 (2007).
52. N.P. Padture, K.W. Schlichting, T. Bhatia, A. Ozturk, B. Cetegen, E.H. Jordan, M. Gell, S. Jiang, T.D. Xiao, P.R. Strutt, E. Garcia, P. Miranzo, M.I. Osendi, *Acta Mater.* **49**, 2251 (2001).
53. S. Krämer, J.Y. Yang, C.G. Levi, *J. Am. Ceram. Soc.* **91** (2), 576 (2008).
54. J.M. Drexler, C.H. Chen, A.D. Gledhill, K. Shinoda, S. Sampath, N.P. Padture, *Surf. Coat. Technol.* **206**, 3911 (2012).
55. R.G. Wellman, J.R. Nicholls, *Tribol. Int.* **41**, 657 (2008).
56. R.V. Hillery, B.H. Pilsner, R.L. McKnight, T.S. Cook, M.S. Hartle, "Thermal Barrier Coating Life Prediction Model Development" (NASA CR 180807, General Electric, 1988).
57. E. Zaleski, R.W. Jackson, C. Ensslen, C.G. Levi, *8th International Symposium on High Temperature Corrosion and Protection of Materials (HTCPM8)* (Les Embiez, France, 2012).
58. J.M. Drexler, A. Aygun, D. Li, R. Vaßen, T. Steinke, N.P. Padture, *Surf. Coat. Technol.* **204** (16–17), 2683 (2010).
59. R.W. Jackson, E.M. Zaleski, M.R. Begley, C.G. Levi, in *International Conference on Metallurgical Coatings and Thin Films* (San Diego, CA, 2012).
60. M.D. Novak, F.W. Zok, *Rev. Sci. Instrum.* **82** (115101) (2012).
61. NRC, "Integrated Computational Materials Engineering: A Transformational Discipline for Improved Competitiveness and National Security" (9780309119993, The National Academies Press, Washington, DC, 2008). □